Synthesis, Characterization, and Preliminary Oxygenation Studies of Benzyl- and Ethyl-Substituted Pyridine Ligands of Carboxylate-Rich Diiron(II) Complexes

*Emily C. Carson and Stephen J. Lippard**

Massachusetts Institute of Technology, Cambridge, MA 02139

RECEIVED DATE August 00, 2005

Table S1. Summary of X-ray Crystallographic Data

	2	**3**·$C_4H_{10}O$	**5**
Empirical Formula	$Fe_2C_{108}H_{88}N_2O_8Cl_2$	$Fe_2C_{106}H_{112}N_2O_9$	$Fe_2C_{110}H_{94}N_2O_8$
Formula Weight	1724.40	1729.64	1683.57
Space Group	Pbca	$P\bar{1}$	$P2_1/c$
a, Å	13.751(3)	14.516(3)	13.774(3)
b, Å	23.133(5)	17.236(4)	23.088(5)
c, Å	27.455(6)	20.031(5)	14.488(3)
α, deg		115.140(3)	
β, deg		91.959(4)	107.498(4)
γ, deg		93.572(4)	
V, $Å^3$	8734(3)	4517.8(18)	4394.4(15)
Z	4	2	2
ρ_{calc}, g/cm^3	1.311	1.271	1.272
T, ºC	-100	-100	-100
μ(Mo Kα), mm^{-1}	0.455	0.383	0.392
θ limits, deg	1.88 – 27.50	1.74 – 26.37	1.78 – 26.38
total no. of data	72872	36881	28010
no. of unique data	9955	18153	7686
no. of params	554	1134	550
Goodness-of-fit on F^2	1.320	1.029	1.029
R1[a]	0.0738	0.0423	0.0634
wR^2[b]	0.1684	0.1096	0.1191
max, min peaks, $e/Å^3$	0.731, -0.493	0.688, -0.358	0.357, -0.313

[a] $R1 = \Sigma||F_o|-F_c||/\Sigma|F_o|$. [b] $wR^2 = \{\Sigma[w(F_o^2-F_c^2)^2]/\Sigma[w(F_o^2)^2]\}^{1/2}$.

Table S1. Continued

	6·2.5CH_2Cl_2	**7**	**8**	**9**
Empirical Formula	$Fe_2C_{101}H_{92}N_2O_8Cl_5$	$Fe_2C_{98}H_{86}N_2O_8$	$Fe_2C_{98}H_{86}N_2O_8$	$Fe_2C_{90}H_{62}N_2O_8F_8$
Formula Weight	1750.72	1531.39	1531.39	1563.12
Space Group	$P2_1/c$	$P\bar{1}$	$P2_1/c$	$P\bar{1}$
a, Å	15.219(2)	12.311(3)	10.775(3)	12.2612(16)
b, Å	10.8186(16)	13.322(3)	24.890(8)	13.3582(17)
c, Å	29.434(4)	14.608(3)	15.118(5)	23.981(3)
α, deg		115.544(3)		84.355(2)
β, deg	117.387(6)	108.042(4)	106.178(6)	86.811(2)
γ, deg		98.087(4)		67.916(2)
V, $Å^3$	4303.1(10)	1947.5(8)	3894(2)	3621.2(8)
Z	2	1	2	2
ρ_{calc}, g/cm^3	1.351	1.306	1.306	1.434
T, ºC	-100	-100	-100	-100
μ(Mo Kα), mm^{-1}	0.553	0.434	0.434	0.484
θ limits, deg	2.04 – 26.38	1.74 – 26.37	1.62 – 26.39	1.65 – 26.37
total no. of data	34613	16083	31640	29709
no. of unique data	8807	7841	7957	14571
no. of params	583	500	500	991
Goodness-of-fit on F^2	1.206	1.224	1.314	1.061
$R1^a$	0.0894	0.0533	0.0734	0.0552
wR^{2b}	0.1886	0.1317	0.1467	0.1237
max, min peaks, $e/Å^3$	0.952, -0.664	0.865, -0.225	1.058, -0.497	0.495, -0.324

$^a R1 = \Sigma||F_o|-|F_c||/\Sigma|F_o|$. $^b wR^2 = \{\Sigma[w(F_o^2-F_c^2)^2]/\Sigma[w(F_o^2)^2]\}^{1/2}$.

Table S2. A Comparison of Fe···Fe and Fe–O Distances in Carboxylate-Bridged Diiron(II) Windmill Structures with Their Coordination Number.

	Coordination Number	Fe···Fe	$Fe–O_{av}$	$Fe–O_L$
1 (Fe1)	4	4.2380(9)	1.999(2)	2.463(2)
1 (Fe2)	5	4.6052(9)	2.033(2)	2.281(2)
2	5	4.3908(11)	2.013(2)	2.308(2)
5	5	4.0656(10)	2.016(3)	2.214(2)
6	4	4.3361(12)	1.998(3)	2.517(3)
7	4	4.0861(10)	1.9714(17)	2.715(2)
8	5	4.1542(14)	2.068(3)	2.323(3)
9 (Fe1)	5	4.4830(10)	2.025(2)	2.225(2)
9 (Fe2)	5	4.4434(10)	2.002(2)	2.330(2)

Captions for Supporting Figures

Figure S1. Top: ORTEP drawing of $[Fe_2(\mu\text{-}O_2CAr^{Tol})_2(O_2CAr^{Tol})_2(2\text{-Bnpy})_2]$ (**1**) illustrating 50% probability thermal ellipsoids for all non-hydrogen atoms. Bottom: Drawing in which the aromatic rings of the $^{-}O_2CAr^{Tol}$ ligands are omitted for clarity.

Figure S2. Top: ORTEP drawing of $[Fe_2(\mu\text{-}O_2CAr^{Tol})_2(O_2CAr^{Tol})_2(2\text{-(4-ClBn)py})_2]$ (**2**) illustrating 50% probability thermal ellipsoids for all non-hydrogen atoms. Bottom: Drawing in which the aromatic rings of the $^{-}O_2CAr^{Tol}$ ligands are omitted for clarity.

Figure S3. Top: ORTEP drawing of $[Fe_2(\mu\text{-}O_2CAr^{Tol})_4(4\text{-Bnpy})_2]$ (**3**) illustrating 50% probability thermal ellipsoids for all non-hydrogen atoms. Bottom: Drawing in which the aromatic rings of the $^{-}O_2CAr^{Tol}$ ligands are omitted for clarity.

Figure S4. Top: ORTEP drawing of $[Fe_2(\mu\text{-}O_2CAr^{Tol})_2(O_2CAr^{Tol})_2(2\text{-Bnan})_2]$ (**5**) illustrating 50% probability thermal ellipsoids for all non-hydrogen atoms. Bottom: Drawing in which the aromatic rings of the $^{-}O_2CAr^{Tol}$ ligands are omitted for clarity.

Figure S5. Top: ORTEP drawing of $[Fe_2(\mu\text{-}O_2CAr^{Tol})_2(O_2CAr^{Tol})_2(2\text{-Etpy})_2]$ (**6**) illustrating 50% probability thermal ellipsoids for all non-hydrogen atoms. Bottom: Drawing in which the aromatic rings of the $^{-}O_2CAr^{Tol}$ ligands are omitted for clarity.

Figure S6. Top: ORTEP drawing of $[Fe_2(\mu\text{-}O_2CAr^{Tol})_2(O_2CAr^{Tol})_2(3\text{-Etpy})_2]$ (**7**) illustrating 50% probability thermal ellipsoids for all non-hydrogen atoms. Bottom: Drawing in which the aromatic rings of the $^{-}O_2CAr^{Tol}$ ligands are omitted for clarity.

Figure S7. Top: ORTEP drawing of $[Fe_2(\mu\text{-}O_2CAr^{Tol})_2(O_2CAr^{Tol})_2(4\text{-Etpy})_2]$ (**8**) illustrating 50% probability thermal ellipsoids for all non-hydrogen atoms. Bottom: Drawing in which the aromatic rings of the $^{-}O_2CAr^{Tol}$ ligands are omitted for clarity.

Figure S8. Top: ORTEP drawing of $[Fe_2(\mu\text{-}O_2CAr^{4\text{-FPh}})_2(O_2CAr^{4\text{-FPh}})_2(2\text{-Etpy})_2]$ (**9**) illustrating 50% probability thermal ellipsoids for all non-hydrogen atoms. Bottom: Drawing in which the aromatic rings of the $^{-}O_2CAr^{4\text{-FPh}}$ ligands are omitted for clarity.

Figure S9. Mössbauer spectrum (experimental data (|), calculated (–)) recorded at 4.2 K for solid sample of $[Fe_2(\mu\text{-}O_2CAr^{Tol})_2(O_2CAr^{Tol})_2(2\text{-Bnpy})_2]$ (**1**).

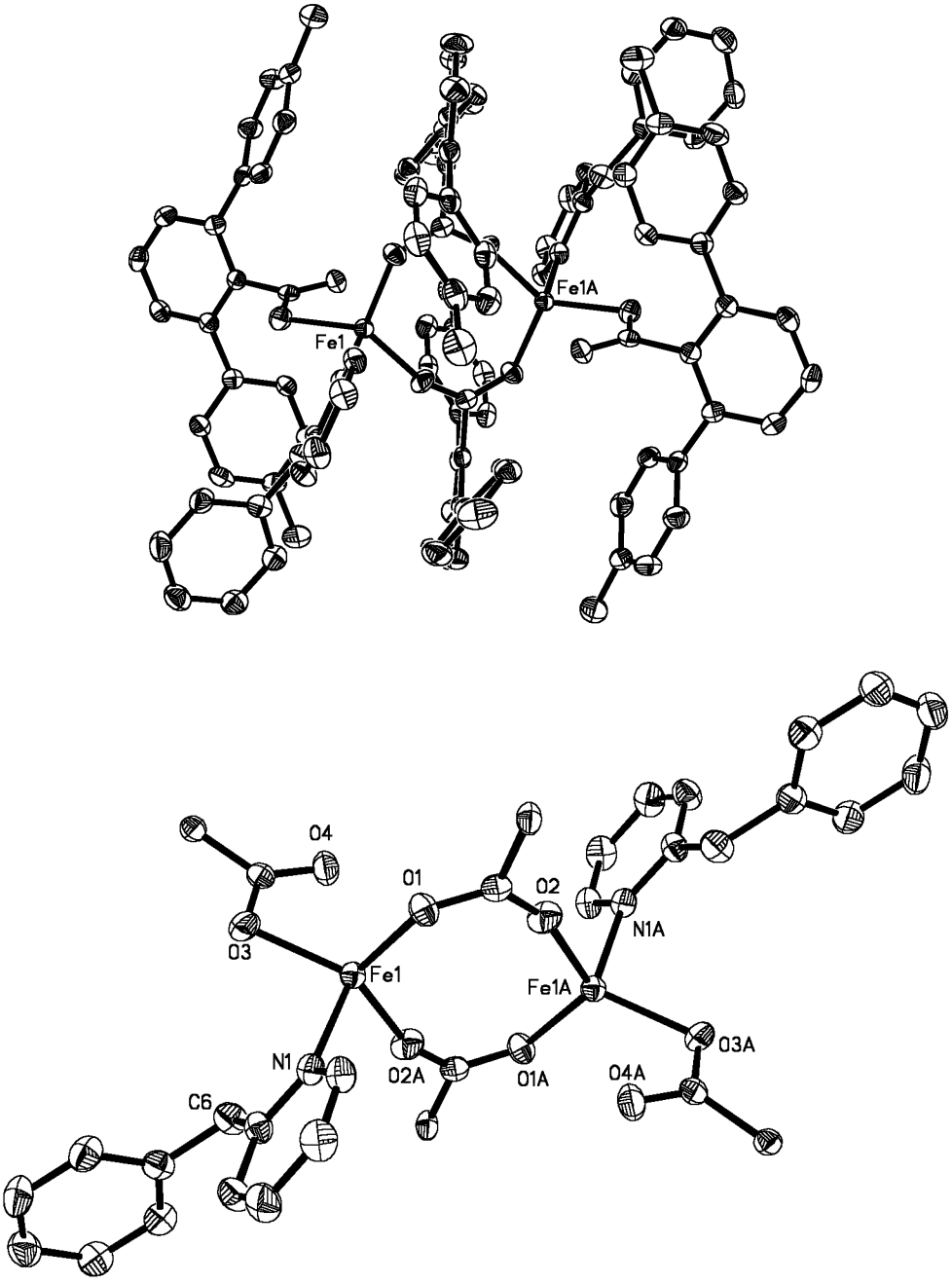

Figure S1. Carson and Lippard

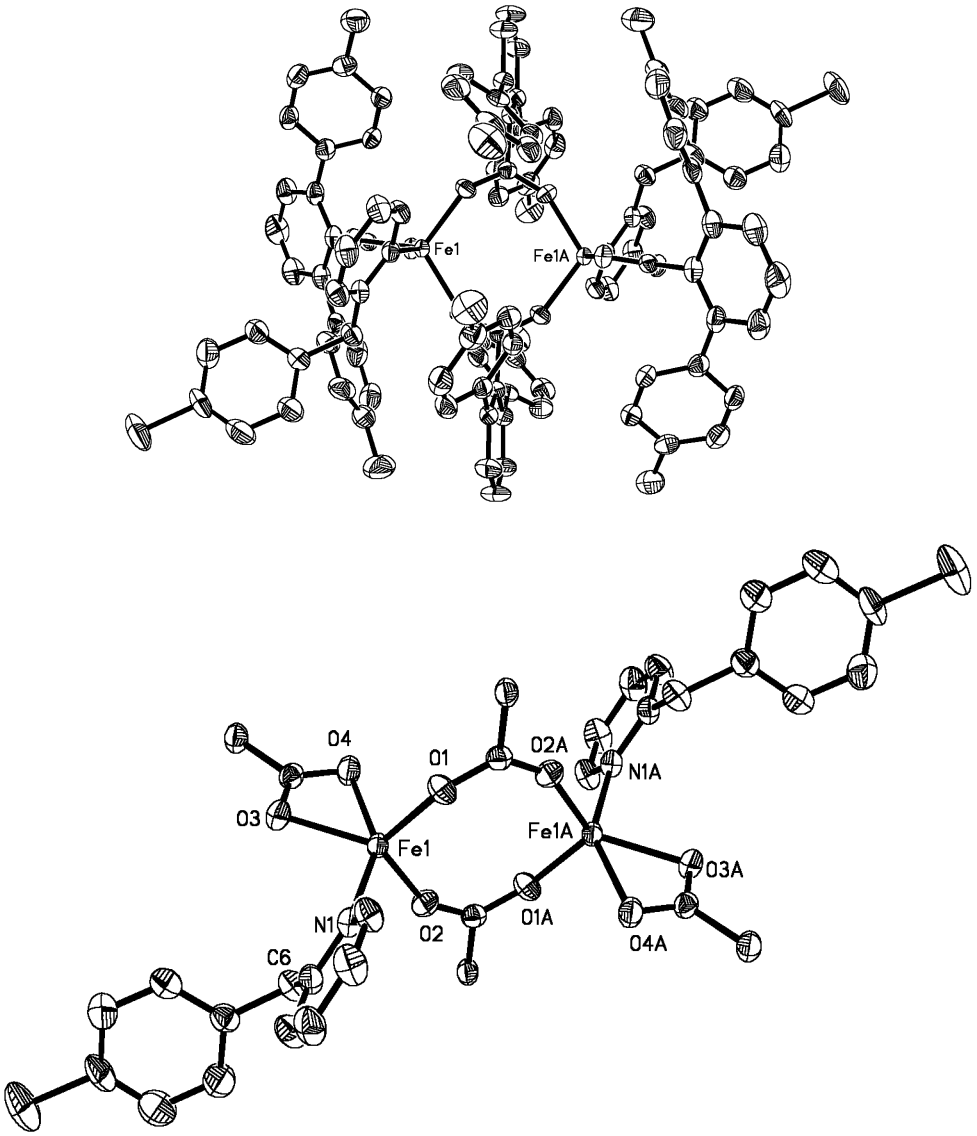

Figure S2. Carson and Lippard

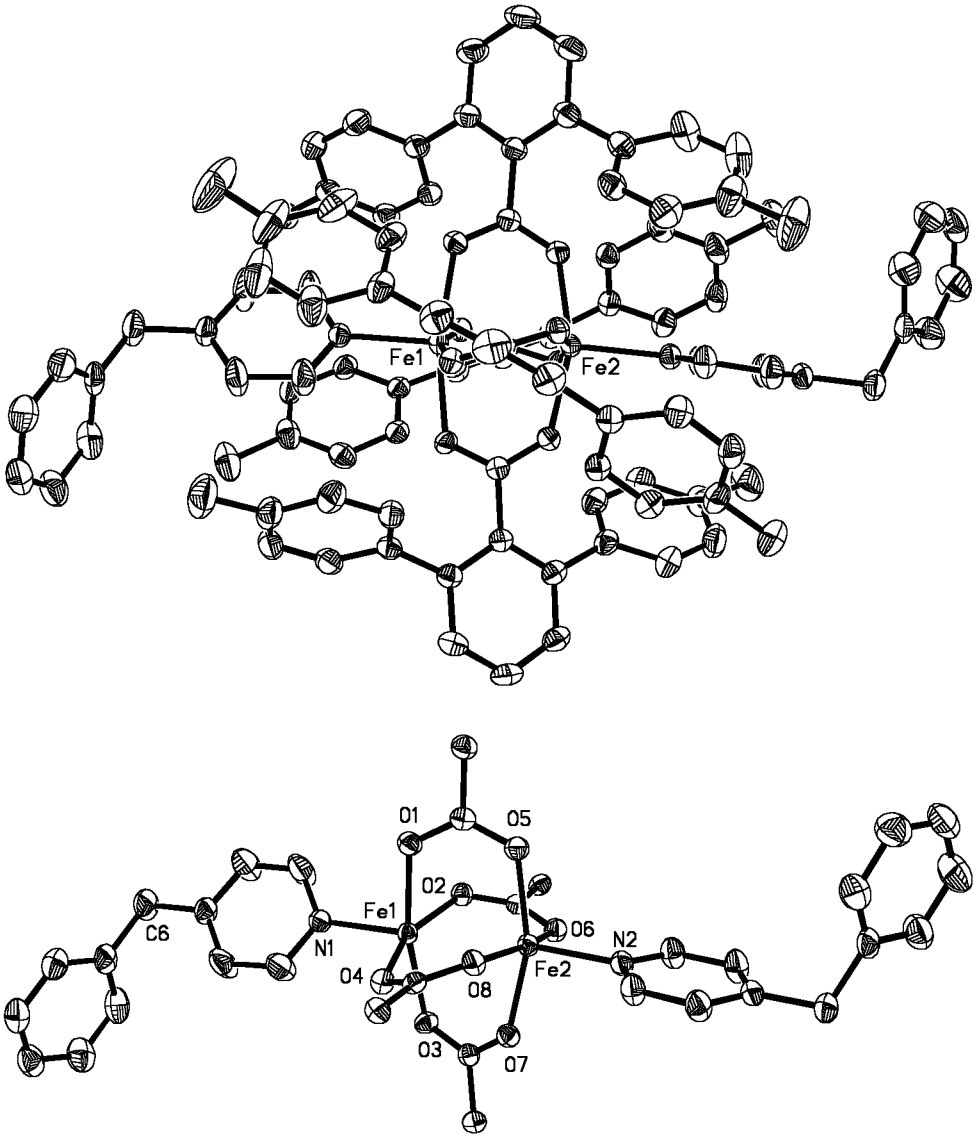

Figure S3. Carson and Lippard

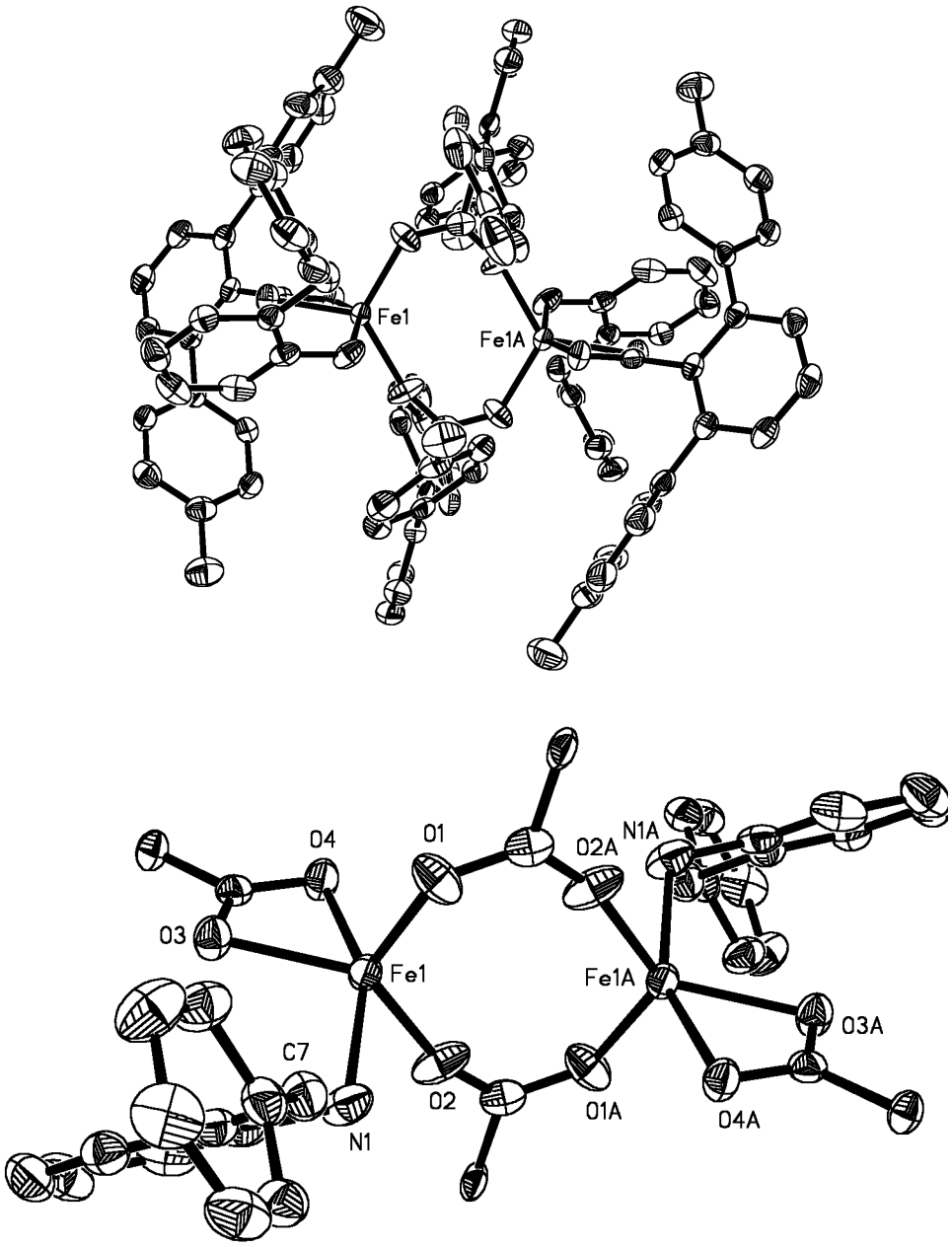

Figure S4. Carson and Lippard

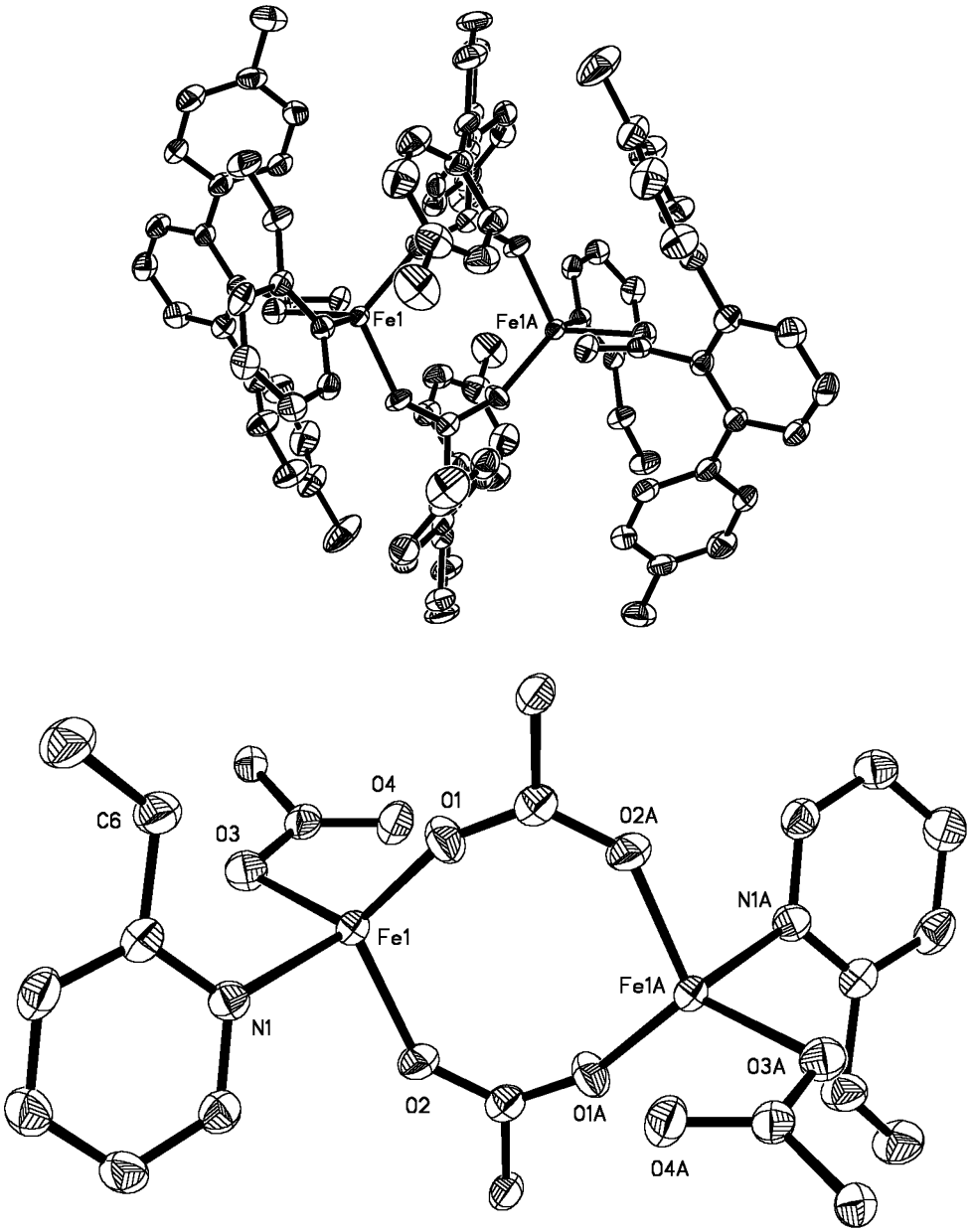

Figure S5. Carson and Lippard

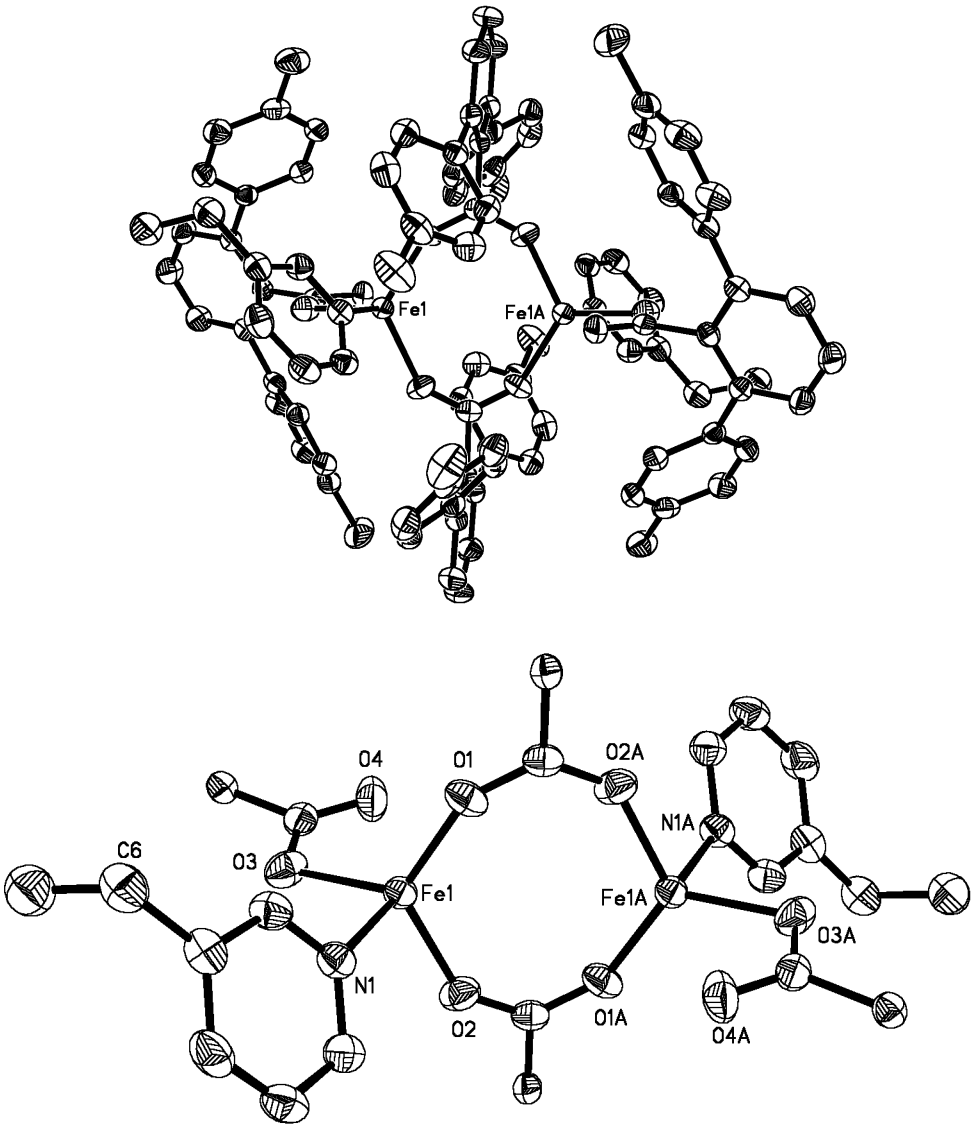

Figure S6. Carson and Lippard

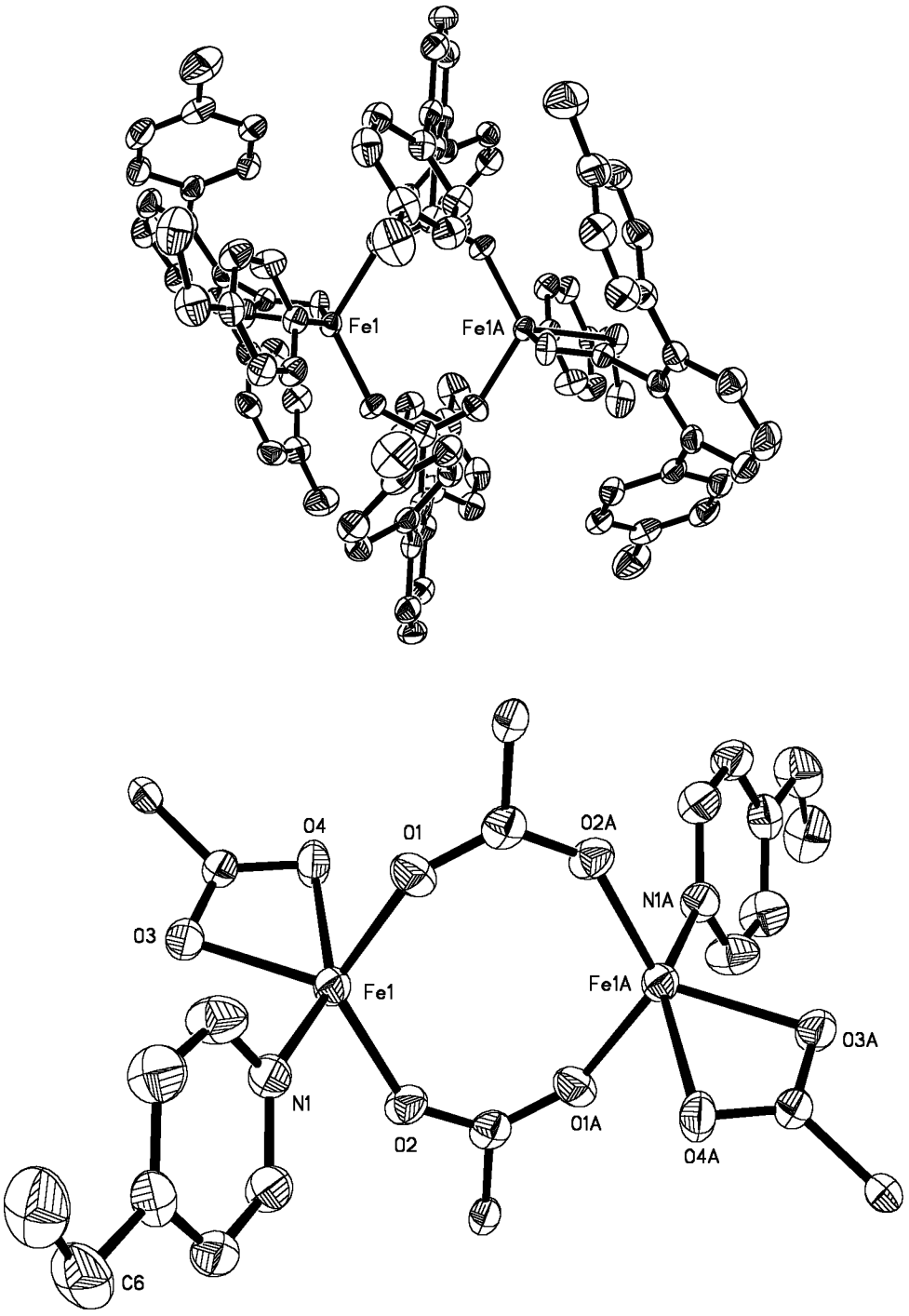

Figure S7. Carson and Lippard

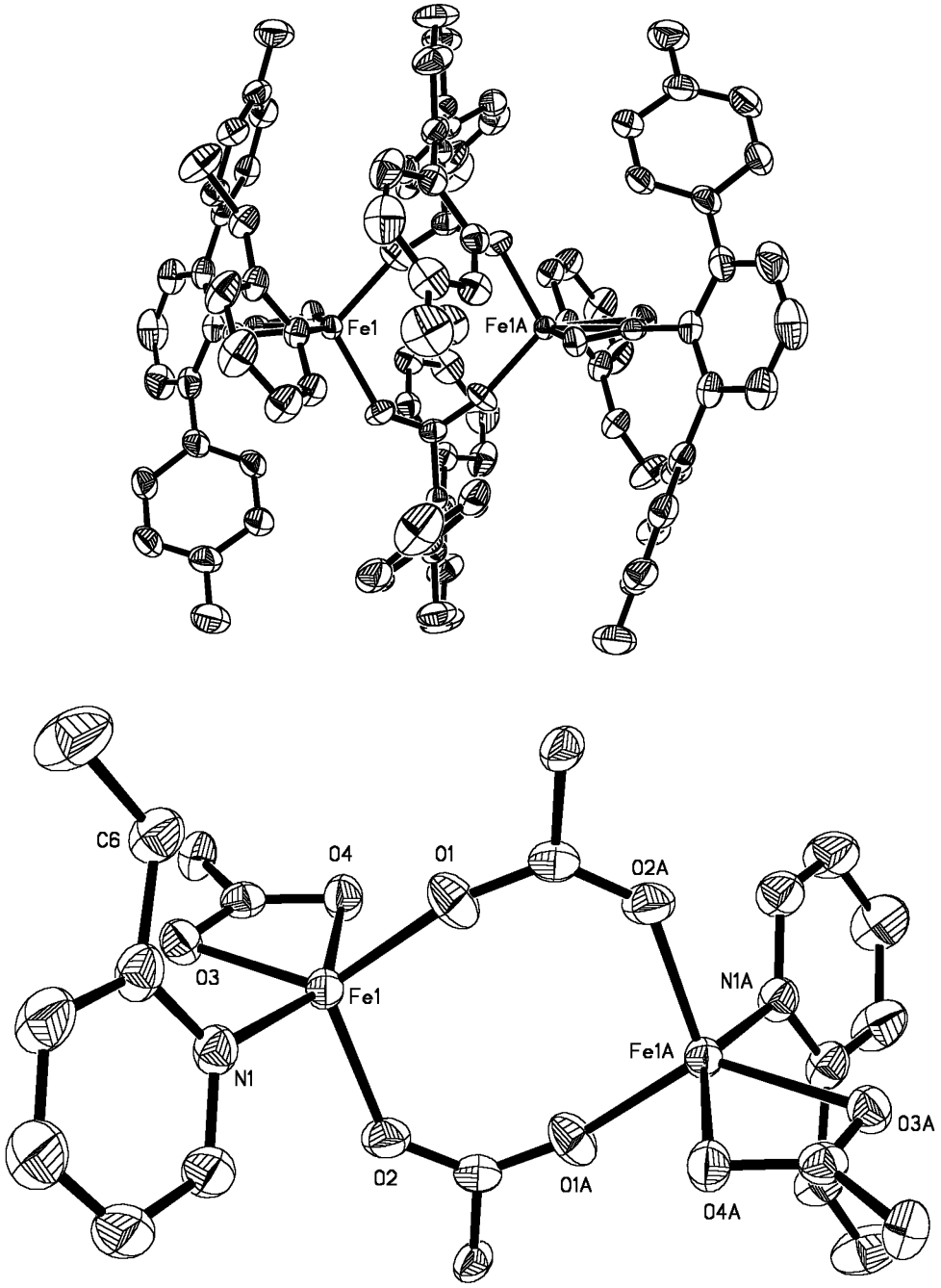

Figure S8. Carson and Lippard

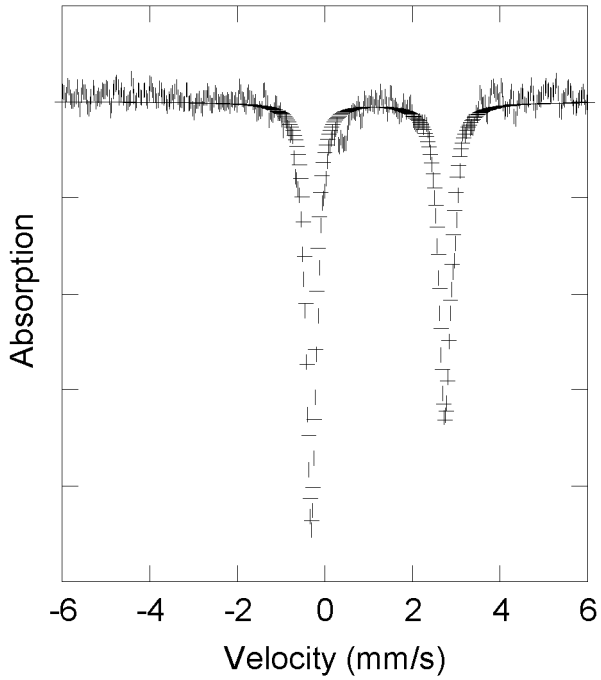

Figure S9. Carson and Lippard